Stand age estimation of rubber (*Hevea brasiliensis*) plantations using an integrated pixel- and object-based tree growth model and annual Landsat time series

Gang Chen[a,*], Jean-Claude Thill[b], Sutee Anantsuksomsri[c], Nij Tontisirin[d], Ran Tao[e]

[a] Laboratory for Remote Sensing and Environmental Change (LRSEC), Department of Geography and Earth Sciences, University of North Carolina at Charlotte, USA
[b] Department of Geography and Earth Sciences, University of North Carolina at Charlotte, USA
[c] Department of Urban and Regional Planning, Chulalongkorn University, Thailand
[d] Faculty of Architecture and Planning, Thammasat University, Thailand
[e] Spatial Sciences Institute, University of Southern California, USA

ARTICLE INFO

ABSTRACT

Rubber (*Hevea brasiliensis*) plantations are a rapidly increasing source of land cover change in mainland Southeast Asia. Stand age of rubber plantations obtained at fine scales provides essential baseline data, informing the pace of industrial and smallholder agricultural activities in response to the changing global rubber markets, and local political and socioeconomic dynamics. In this study, we developed an integrated pixel- and object-based tree growth model using Landsat annual time series to estimate the age of rubber plantations in a 21,115 km^2 tri-border region along the junction of China, Myanmar and Laos. We produced a rubber stand age map at 30 m resolution, with an accuracy of 87.00% for identifying rubber plantations and an average error of 1.53 years in age estimation. The integration of pixel- and object-based image analysis showed superior performance in building NDVI yearly time series that reduced spectral noises from background soil and vegetation in open-canopy, young rubber stands. The model parameters remained relatively stable during model sensitivity analysis, resulting in accurate age estimation robust to outliers. Compared to the typically weak statistical relationship between single-date spectral signatures and rubber tree age, Landsat image time series analysis coupled with tree growth modeling presents a viable alternative for fine-scale age estimation of rubber plantations.

1. Introduction

Rubber trees (*Hevea brasiliensis*) produce latex, serving as the primary source of natural rubber. Unique properties of elasticity, resilience, and toughness (Payne, 1962) have made rubber an ideal polymer for a wide variety of applications in transportation (e.g., tires), industrial (e.g., silicone sheets), consumer (e.g., clothing), and medical sectors (e.g., tubing and cord). The ever expanding demand for rubber products has significantly boosted rubber cultivation, mostly in mainland Southeast Asia, where more than 1.5 million ha of land were converted to rubber plantation from 2003 to 2010 (Kumagai et al., 2015). While global rubber prices weakened following the 2008 economic recession, they were more recently observed to bounce back in tandem with increased demand in leading rubber markets, such as China (IndexMundi, 2017). Today's rubber plantations have expanded rapidly to non-traditional rubber tree-growing regions, including

southern China, eastern Myanmar, northern Laos, northeast Thailand, and Cambodia (Li and Fox, 2012). Such fast pace of land-cover conversion provides the countries, their agribusiness, and local farmers with high economic returns (Smajgl et al., 2015). However, financial gains have come with certain costs. The rubber industry has been found to cause substantial carbon emissions, reduced water and food security, biodiversity loss, and decreased provision of ecosystem services (Mann, 2009; Ziegler et al., 2009; Yi et al., 2014; Blagodatsky et al., 2016; Giambelluca et al., 2016). Other intertwined issues include stress on the national land tenure system, military/business land grabbing, ethnic strife, and territorial control (Woods, 2012).

Estimating the age of rubber plantations provides essential baseline data for understanding the role of rubber boom in shaping the agricultural, forest and urban landscapes of mainland Southeast Asia. Particularly, countries in this region have diverse political and socioeconomic statuses. The timing of rubber cultivation informs us on the

variation in rubber policies and plantation activities in response to the changing global rubber markets. Accurate age estimation of rubber plantations further facilitates agricultural land management by complementing the national and regional land use maps (e.g., GlobeLand30; Chen et al., 2014b), which typically contain broad land use types without detailed information about major cash crop in the region. The majority of remote sensing-based rubber tree mapping activities has been conducted fairly recently with an emphasis on estimating the areal extent of rubber plantations. Ideally, if the spatial distribution of rubber plantations is accurately extracted on an annual basis, the age of rubber trees becomes readily available. Directly linking single-date spectral signatures with land-cover types (including rubber tree cover) remains classic, and was confirmed with moderate success in several projects (e.g., Li and Fox, 2011; Zhai et al., 2012; Trisasongko, 2017). However, rubber trees could expose strong spectral similarities with natural forests, croplands or shrublands during certain seasons (Li and Fox, 2012; Dong et al., 2012). Without fully understanding their phenological traits, practitioners run the risk of misclassifying rubber with other species growing in the same area.

To address this challenge, Dong et al. (2012) compared the intra-annual variability of three MODIS indices, namely NDVI (Normalized Differential Vegetation Index), EVI (Enhanced Vegetation Index), and LSWI (Land Surface Water Index) among rubber, paddy rice cropland, and evergreen forest. Superior mapping performance was achieved by applying a thresholding approach to two averaged NDVI images from the rubber tree growing season (March to October) and non-growing season (October to March of next year), respectively. Instead of using two NDVI images, Li and Fox (2012) imported a total of 29 MODIS semimonthly NDVI composites for an entire year to the Mahalanobis distance classifier, and successfully extracted both young (< 4 years old) and mature (≥ 4 years old) rubber trees. However, the temporal profiles of spectral signatures from MODIS dense time series possibly contain atmospheric noises and gaps (e.g., caused by clouds). Senf et al. (2013) fit non-linear least squares models to the MODIS raw time series, and extracted the simulated phenological metrics (base values of season, start of season, maximum of season, and end of season) to be used in a Random Forest classification.

While the dense time series from MODIS facilitates vegetation phenological analysis, its coarse spatial resolution (250 m) poses a challenge for delineating small-size rubber plantations managed by smallholders. In fact, smallholders predominate rubber production in several large rubber producing countries and regions. In Thailand, for instance it is estimated that 90 percent of rubber is produced by smallholders (Fox and Castella, 2013). With a finer spatial resolution, Landsat (30 m) imagery has demonstrated success in several rubber mapping projects (e.g., Chen et al., 2012; Dong et al., 2013; Grogan et al., 2015). For example, Dong et al. (2013) discovered a unique phenological phase (late March to April) in south China, where rubber trees underwent rapid foliation and canopy recover causing high spectral reflectance in the near-infrared region of the spectrum. With such strategy, the spatiotemporal dynamics of rubber plantations may be captured if high-quality Landsat time series are available on an annual basis. It alleviates the need for intra-annual dense time series, which is challenging to acquire in cloud-prone tropical and sub-tropical mainland Southeast Asia. However, high-quality data does not necessarily lead to an accurate estimation of rubber tree age. Previous efforts were primarily devoted to extracting the areal extents of mature rubber trees (typically 6–7 years or older) with closed canopies [e.g., Chen et al. (2012); Dong et al. (2012; 2013); Li and Fox (2012)]. The spectral characteristics of open-canopy, young rubber stands are often affected by the spectral 'noises' from background land cover, e.g., bare soil or vegetation, causing high mapping errors.

The main objective of this study is to develop a fine-scale, remote sensing approach to improve the estimation accuracy of the stand age of rubber plantations. Here, we propose an integrated pixel/object-based tree growth model using annual Landsat time series. The model is

developed with two main considerations. First, we capitalize on Geographic Object-based Image Analysis (GEOBIA; Blaschke et al., 2014; Chen et al., 2018; Chen and Weng, 2018) using image-objects (aggregates of pixels) to mitigate the effect of background spectral noises typically occurring in young rubber stands. Since image-objects from different dates vary in geometry even if they represent the same geographic features (Chen et al., 2014a,b), we integrate pixel- and object-based image analysis facilitating the comparison among multi-temporal image-objects for constructing an improved Landsat time series database. Second, the cash crop rubber trees expose an annually fast growing pattern, which differs from that of natural forests and many other crop types (e.g., paddy rice). Fitting a tree growth model to the improved time series database provides a potential means to capture the relatively unique rubber tree growth trajectories, from which stand age can be determined. Such integration of remote sensing and a long-term tree growth model differs from previous efforts that mainly rely on spectral and short-term phenological traits of rubber trees.

2. Methods

2.1. Study area

The selected study area (centered at 21°25′50″N, 100°55′00″E) is a tri-border region along the junction of China, Myanmar and Laos (Fig. 1). It covers part of Yunnan Province (China), Shan State (Myanmar), and Luang Namtha Province (Laos), with a total areal size of 21,115 km^2. The region features tropical and sub-tropical monsoon climate, with an annual mean temperature of approximately 25°Celsius, and annual precipitation ranging from 1000 to 2400 mm (Liu et al., 2013). Slopes and drainage dissect the rugged landscape of the region with elevations ranging from 267 m to 2555 m above sea level. The area also harbors exceptionally high levels of biodiversity, with more than 5000 flowering plant and fern species (Zomer et al., 2014). Forests mainly include tropical rainforests, tropical monsoon forests, and sub-tropical monsoon evergreen broadleaf forests (Liu et al., 2013).

Rubber plantations have been expanding rapidly in the region gradually replacing ecologically important secondary forests and traditional upland agriculture and swidden farming (Li and Fox, 2012; Liu et al., 2016). The regional rubber farms were initially established in the 1950s in Yunnan, China, where natural rubber was considered as an important strategic national resource by the Chinese central government (Smajgl et al., 2015). Since the 1990s, rubber plantations have risen in the neighboring Shan State (Myanmar) and Luang Namtha Province (Laos). The pace of rubber cultivation was particularly rapid in the first decade of the 21st century, mainly driven by globally strong rubber markets and the growing demand from major rubber consumers, e.g., China, India, United States and Japan (Alton et al., 2005). In Xishuangbanna (south of Yunnan) alone, rubber plantations doubled from 2007 to 2010 (Xu et al., 2013). Some parts of the study area in Myanmar and Laos have also experienced a transition from cultivating opium poppy to rubber trees, which was supported by the Opium Poppy Substitution Planting programme (Liu et al., 2016). To date, the decadal, fine-scale rubber expansion patterns remain to be well estimated, preventing a timely analysis of the response of local rubber industry to various policies, socioeconomic dynamics, and the fluctuation in the global rubber market.

2.2. Data and pre-processing

The study area encompassed most of a single Landsat image footprint (path: 130; row: 45). Landsat time series were acquired for a period of 15 years (2001–2015). Within this time window, rubber price quickly surged to an all-time high and dropped to a decade low (IndexMundi, 2017). We aimed to analyze the rate and spatiotemporal pattern of rubber plantation expansion during the same window. Each year, only one image scene was used and downloaded from the U.S.
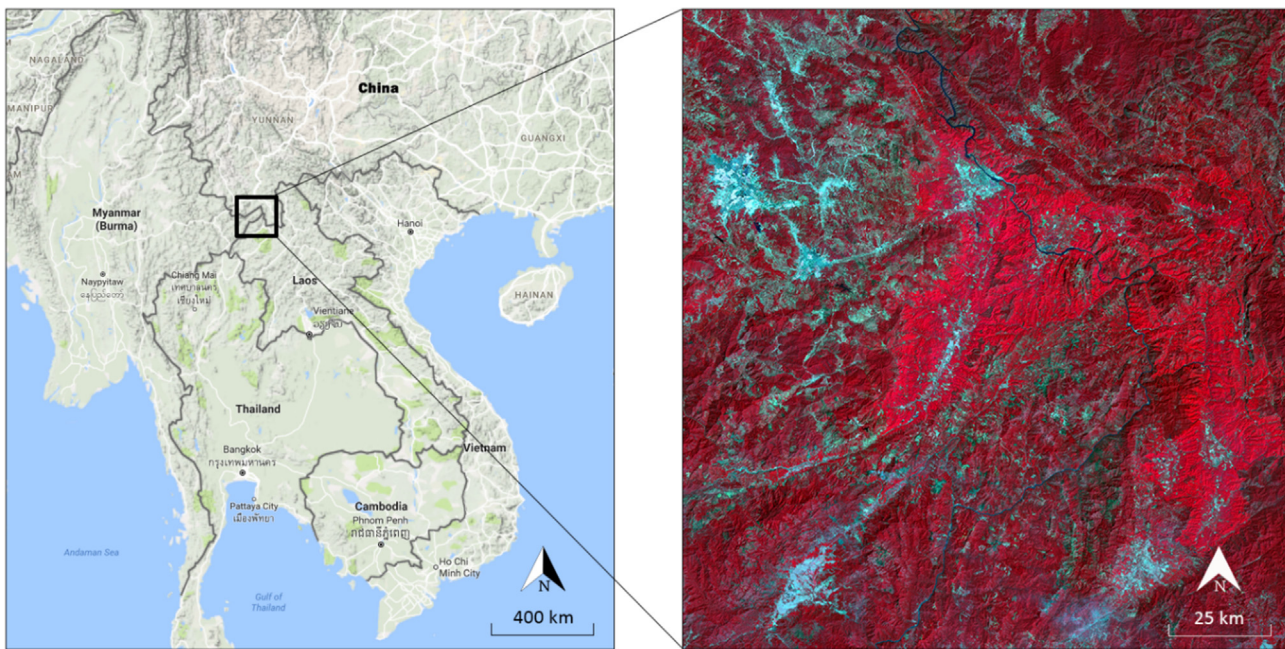
Fig. 1. Mainland Southeast Asia (left) and a Landsat 8 false-color composite (red: near infrared band, green: red band, blue: green band) of the study area (right), which is a tri-border region along the junction of China, Myanmar and Laos. (For interpretation of the references to colour in this figure legend, the reader is referred to the web version of this article.)

Geological Survey data portal (http://glovis.usgs.gov). We analyzed the phenological traits of local vegetation and found a unique dry-season phase (March to April), when the rapid foliation of rubber trees led to higher NDVI values than many other plant types, which was relatively consistent with the findings by Li and Fox (2012) and Dong et al. (2013). In this study, all the annual images were acquired within or close to this time window. The data were collected by three Landsat satellites: Landsat 5 (L5), Landsat 7 (L7) and Landsat 8 (L8). More specifically, 2001 (sensor: L7; Julian day: 108), 2002 (L7; 095), 2003 (L7; 098), 2004 (L5; 061); 2005 (L5; 047), 2006 (L5; 066), 2007 (L5; 085), 2008 (L5; 088), 2009 (L5; 106), 2010 (L5; 045), 2011 (L5; 080), 2012 (L7; 059,075,107), 2013 (L7; 061,077,093), 2014 (L8; 104), and 2015 (L8; 075). For the years 2012 and 2013, we gap-filled the Landsat 7 SLC-off data through mosaicking three images per year, simply filling the missing pixel values with the available values from the other images obtained from the same dry season. This study used the surface reflectance products derived from the raw Landsat imagery, which were geometrically, radiometrically and topographically corrected by NASA before being made available online.

The ground-truth data were collected mainly through photo interpretation of the Google Earth (Mountain View, California, USA) high-spatial resolution satellite imagery. We extracted a total of 300 sample points. To ensure a balanced representation of rubber plantations and other land cover types, a random stratified sampling strategy was used with approximately 50% of the samples having rubber plantations within a 15-year time frame (consistent with our study time window); while the remainder did not. We slightly adjusted the location of rubber samples to include a range of ages from young, middle-age to mature plantations. This was completed to avoid a potential bias to certain age groups during model calibration and validation. To reduce uncertainties in photo interpretation, we visited some local regions in Myanmar and Thailand, which had similar climate and rubber cultivation patterns as those in our study area. More specifically, we compared rubber plantations from the local regions and those in the corresponding Landsat and high-resolution images. The experience of understanding the plantation-image relationship was extended to interpreting the images in our study area. Fig. 2 shows three field photos corresponding to the three stages of rubber tree growth from an open-

canopy, young stand (a), a middle-age stand (b), to a closed-canopy, mature rubber stand (c).

2.3. Age estimation of rubber plantations

There are three major steps in the proposed model: (a) building yearly NDVI time series, (b) modeling rubber tree growth, and (c) mapping the stand age of rubber plantations. In general, step (a) prepared an improved NDVI time series database using an integrated pixel/object-based approach. The database was used in step (b) for calibrating a rubber tree growth model, which was subsequently applied in step (c) for identifying rubber plantations and the associated stand age across the entire study area. This is now discussed in more detail.

(a) Image-objects were firstly extracted from individual Landsat images in eCognition Developer 8 (Trimble Navigation, Sunnyvale, California, USA). A scale parameter (defining mean object size) of 60 was consistently used to derive image-objects at the small tree patch level. While some tools (e.g., ESP, Drăguţ et al., 2010) have been created to automatically determine scale parameters based on local variance, we still used the trial-and-error exploration with an aim to slightly merge neighboring canopy and soil pixels in the plantation at the young stage. This is because at the young stage, the spectral signatures of rubber tree canopies and background soil often reveal high contrast, causing a single plantation area to be overly segmented if local variance is used. The high variation in the NDVI time series will make fitting tree growth model a challenging task (see next step). The parameters of shape and compactness were set to the software default values of 0.1 (shape) and 0.8 (compactness). We also evaluated other shape and compactness values and obtained similar segmentation results, which is consistent with our previous experience in segmenting forest landscapes (Chen et al., 2015). A sample segmentation result is presented in Fig. 3, in which a rubber tree stand (overlapped with the yellow-boundary image-objects) shows a growth pattern from young (2005), middle-age (2010) to mature (2015). Particularly at the young stage of tree growth as illustrated in the 2005 Landsat image, the spectral variation within the yellow boundary is high, with grey color representing soil and red color indicating vegetation cover. It is therefore challenging to delineate such a young tree stand using the classic

Fig. 2. Field photos showing an open-canopy, young rubber stand (a), a middle-age stand (b), and a closed-canopy, mature stand (photo credit: Gang Chen).
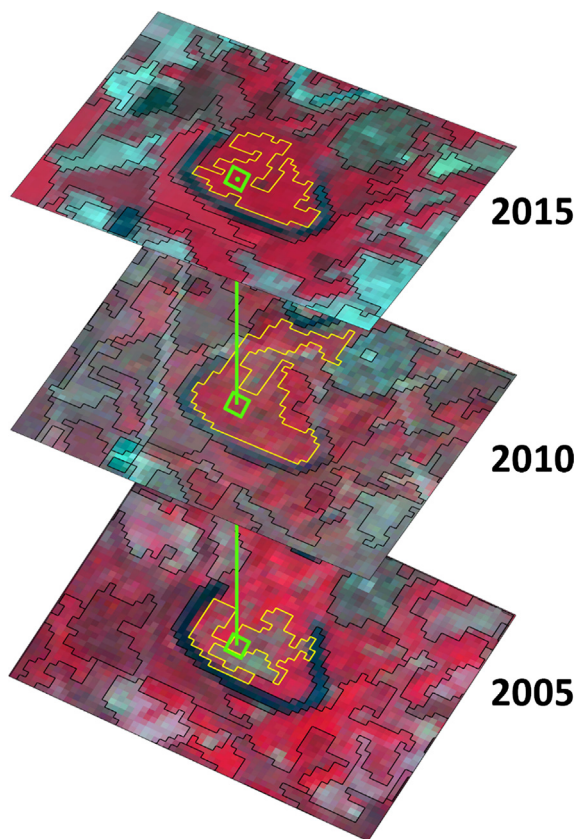

Fig. 3. Image-objects (yellow boundaries) capturing three stages of rubber tree growth, young (2005), middle-age (2010), and mature (2015). Three green grid cells represent pixels covering the same part of a rubber tree stand over years. (For interpretation of the references to colour in this figure legend, the reader is referred to the web version of this article.)

pixel-based approach. In this study, the yearly NDVI values were calculated using the Landsat near-infrared and red reflectance bands, which were averaged at the object level.

To build NDVI time series, we avoided directly comparing multi-temporal image-objects, because these objects demonstrated inconsistent geometries (see yellow-boundary objects in Fig. 3) induced by the change in tree crown density, plantation areal extent, and/or sun-sensor geometry (Chen et al., 2011). Here, the time series was derived from the areas corresponding to individual Landsat pixels (30 × 30 m; see green grid cells in Fig. 3), although we still used the object-based yearly NDVI values derived in the previous paragraph. Such an approach facilitated a straightforward comparison of NDVI values across years, while mitigating the impact of spectral noises particularly from young rubber tree stands.

(b) We modelled annual tree growth using a logarithmic function, with NDVI serving as a proxy of plant productivity. According to our initial experiments, logarithmic function demonstrated superior performance simulating rubber tree growth, as compared to several other types of functions (e.g., linear and exponential).

$$y = a \cdot \ln(x) + b + \varepsilon \tag{1}$$

where y is the age of rubber stand, x is the corresponding NDVI value, a and b are model parameters, ε is the error term. In this study, field surveys and ground-truth data showed that rubber trees grow particularly fast within the first decade of cultivation, and their NDVI values become stable after trees reach maturity. Accordingly, we set a ten-year maximum time window for fitting the model to each of the NDVI time series. A minimum time window of three years was also chosen because the model needed at least three observations to generate meaningful results. Fig. 4 shows an example of NDVI trajectories within a 10-year window from a rubber stand, a natural forest patch, and a non-rubber, paddy rice cropland. The dotted lines are observations extracted from the satellite-based NDVI time series (see Section 2.2). The solid trending lines represent the corresponding fitted plant growth trajectories (using Eq. (1). Generally, rubber plantations in our study area showed steeper slopes of NDVI trajectories (i.e., larger a in Eq. (1) than natural forest stands, non-rubber croplands or shrublands. In addition, land clearing is a common practice prior to rubber cultivation in many areas of Southeast Asia (Simorangkir et al., 2002). The initial value of a rubber NDVI trajectory (i.e., b in Eq. (1) reflected a bare or near-bare ground condition. In the study, the calibration/training of the tree growth model used two thirds of the randomly extracted ground truth samples, while the remainder was used in model validation for accuracy assessment (see Section 2.4). Through calibration, we derived the optimal range of model parameters a and b, which were applied to mapping the stand age of rubber plantations described in the following section.

(c) Mapping the stand age of rubber plantations was performed on NDVI time series at individual pixel locations. We first selected potential candidates as the starting year of rubber tree cultivation, where NDVI values were smaller than 0.4 in the time series. This threshold was chosen to represent bare ground conditions or land covered by low-density vegetation. It was a relaxed threshold used to overestimate rubber plantations. We then fitted the tree growth model to the NDVI time series (Eq. (1) treating each candidate as the cultivation starting year. All the possible time windows, ranging from 3 to 10 years, were used for modeling. In many cases, the maximum time window was less than 10 years, when the candidates were close to the end year of the time series (2015). The candidate was finally chosen as the real starting year of rubber tree cultivation based on two criteria: (i) The model parameters a and b are located in the optimal value range (as described in the previous paragraph), and (ii) the variation of a (slope of the fitted trending line) is small, with the standard deviation value lower than 0.03. Criterion (i) was applied to identify possible rubber plantations, capitalizing on the rapid growth rate of rubber trees (Fig. 4). Criterion (ii) was mainly used to identify 'spurious' candidates within a rubber NDVI time series, typically related to low data quality (e.g., caused by cloud cover). Fig. 5 provides an example of two NDVI trajectories starting from a real candidate (left) and a spurious candidate (right), both from rubber tree stands. The tree growth model was fitted to the NDVI observations using multiple time windows from 3 to 7 years.
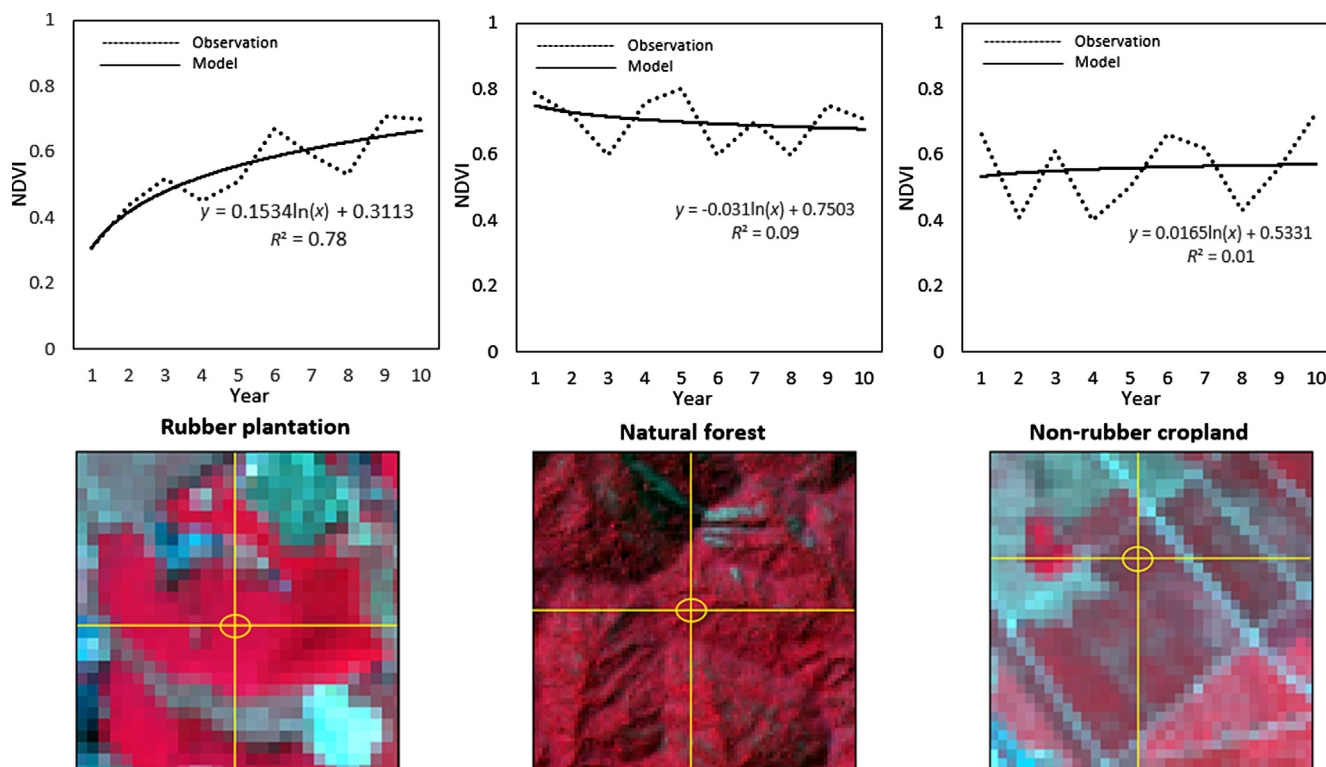
Fig. 4. NDVI yearly trajectories for a rubber tree stand, a natural forest patch, and a non-rubber cropland. Landsat false-color composites (red: near infrared band, green: red band, blue: green band) were used to represent the three types of land cover. (For interpretation of the references to colour in this figure legend, the reader is referred to the web version of this article.)

When the spurious candidate was treated as the starting year, all the fitted tree growth models showed steep slopes, similar to those using the real candidate (Fig. 5). However, the variation of a was high. Because the NDVI value corresponding to the spurious candidate was off the rubber tree growth trajectory, feeding NDVI observations to the model (i.e., testing different time windows) was found to cause high variation. In this study, we used a sample of rubber plantations to train the tree growth model (see sampling and model calibration in the previous section), from which the variation threshold of 0.03 was determined.

2.4. Accuracy assessment and model parameter evaluation

Using one third of the randomly extracted ground truth samples, model performance was evaluated with classic R^2 and RMSE for age estimation, and a confusion matrix and kappa statistic for mapping the spatial distribution of rubber plantations. Please be aware that the proposed model emphasized on the plantations that were initiated within the studied time frame (2001–2015). Rubber trees that were planted prior to 2001 were not considered in this research, and excluded from map accuracy assessment. We further assessed the sensitivity of the tree growth model by adding random errors to NDVI
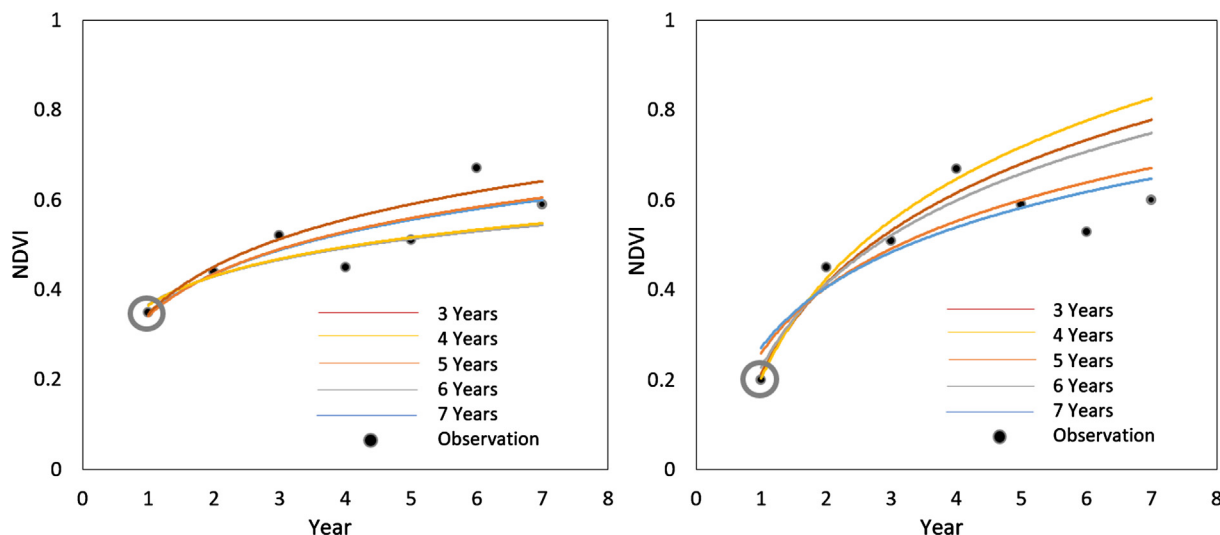

Fig. 5. Yearly NDVI trajectories starting from a real candidate year (left) and a spurious candidate year (right). The tree grow model was fitted to the data in various time windows.
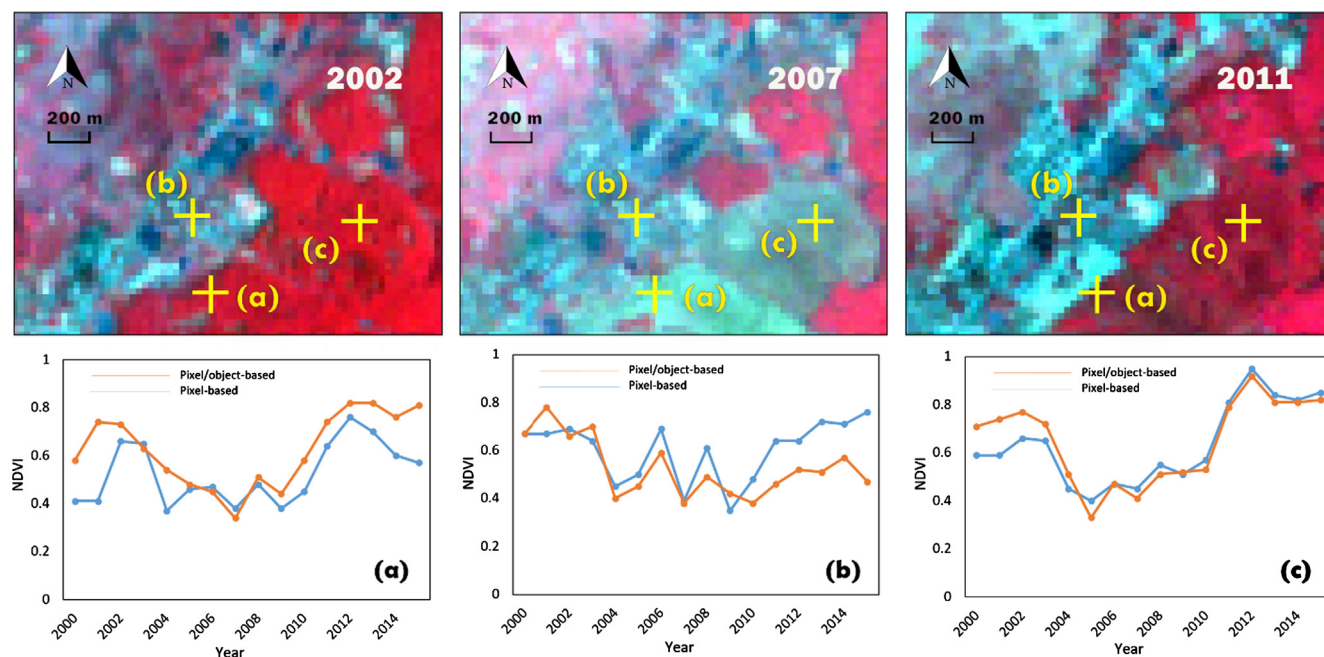
Fig. 6. Comparison of NDVI trajectories extracted from the proposed pixel/object-based *versus* classic pixel-based approach for three sample locations (a), (b) and (c). The three Landsat images show land cover at three sample time steps 2002, 2007 and 2011.

observations. Such analysis was used to understand the robustness of the proposed model to the uncertainties in NDVI values, typically caused by the variation in image acquisition dates and/or inconvenient weather conditions (e.g., cloud or fog cover).

3. Results and discussion

3.1. NDVI trajectories from pixel/object-based versus classic pixel-based image analysis

The rubber plantations in the study area included both large-scale and smallholder farms. In either case, the proposed pixel/object-based approach was found to more effectively reduce spectral noise and to extract NDVI time series with more apparent trajectory patterns than the classic pixel-based image analysis. The size of plantation has no direct impact on the extraction of time series. Although plantations may be smaller than one pixel area (900 sqm), such practices are rare due to the low economic feasibility. Fig. 6 illustrates three sample locations, including two rubber (a and c) and one non-rubber (b) plots. Plots a and c were covered by dense vegetation in 2002 (red color in the NIR-R-G composite), which were erased in around 2007 (grey color representing bare or close-to-bare ground conditions). Within four years, the areas quickly recovered through cultivation of rubber trees as evidenced in the 2011 image. Both a and c represented part of rubber plantations. For plot c, the proposed and the classic image analysis generated similar NDVI change trajectories. As for plot a, the pixel-based analysis resulted in three low NDVI values from 2004, 2007 and 2011, challenging the identification of the real starting year of rubber tree cultivation. In contrast, the pixel/object-based approach resulted in only one valley, and NDVI showed a steadily increasing trajectory after 2007 (Fig. 6). As argued by Dong et al. (2012) and Li and Fox (2012), the spectral characteristics of open-canopy, young rubber stands are likely affected by the noise from background land cover of bare soil or vegetation. Our assessment indicated the benefits of accommodating the neighborhood spectral features (using objects) for mitigating the noise effect. Such benefits also applied to non-rubber stands. For instance, plot b (Fig. 6) was not in a rubber plantation. The neighborhood was covered by sparsely distributed vegetation causing high dynamics of NDVI across the area. The pixel-based analysis produced a strong NDVI upward

trend from 2009 to 2015 (blue color), similar to a rubber tree growth pattern. When the neighborhood (contextual) information was integrated, the NDVI trajectory (orange color) had a gentle gradient of slope, reflecting the actual non-rubber land condition.

3.2. Parameter evaluation of tree growth model

The optimal value range for model parameters *a* and *b* was calculated using the training samples. For our study area, the maximum, minimum, average and standard deviation were found to be 0.34, 0.18, 0.23 and 0.03 for *a*, and 0.38, 0.21, 0.31 and 0.05 for *b*, respectively (Table 1). Parameter *a* reflected the annual rate of tree growth, and showed higher values than those from natural forests and many other croplands. The annual time series analysis addressed the challenge of rubber tree extraction from single-date imagery, where all plants could exhibit similar NDVI values. Although we employed dry-season (March to April) Landsat imagery, which led us to expect higher rubber NDVI values from the rapid foliation of rubber trees, it was still inevitable to discover rubber and non-rubber plants with similar spectral signatures. The tree growth rates (values of *a*) were observed to range from 0.18 to 0.34, possibly caused by the dynamic microclimates in this mountainous region, with elevation changing from 267 to 2555 m. Parameter *b* was equivalent to the background NDVI at the tree age of one. Its values were a reasonable representation of bare ground. The variation in *b* was possibly the result of mixed spectral signatures from soil, grass, shrub and/or crops. In addition, all the rubber tree growth models had relatively strong performance fitting the annual NDVI observations, with R^2 ranging from 0.62 to 0.94 (Table 1).

To evaluate the model's sensitivity to the uncertainties in NDVI observations, we randomly added errors of 5%, 10%, 15%, 20%, 25%,

Table 1
The estimates of tree growth model parameters a and b, and R-squared values.

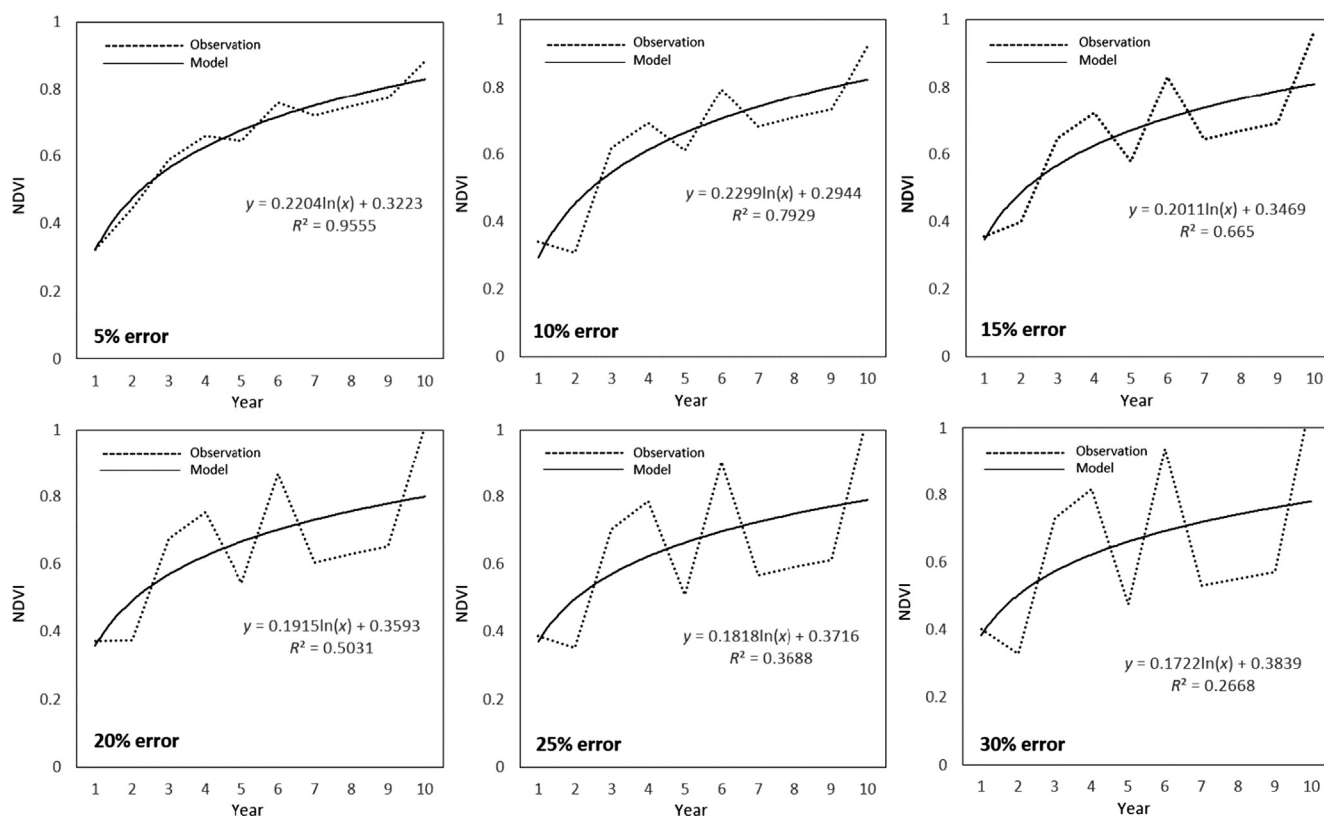| Model	Maximum	Minimum	Average	Standard deviation
Parameter *a*	0.34	0.18	0.23	0.03
Parameter *b*	0.38	0.21	0.31	0.05
R-squared	0.94	0.62	0.80	0.09

Fig. 7. The performance of tree growth model with a series of errors added to all the observations (error levels: 5%, 10%, 15%, 20%, 25%, and 30%).

and 30% to an NDVI time series simulated with the average a (0.23) and b (0.31). For each error level (e.g., 5%), individual NDVI observations were randomly selected to incorporate a positive or negative change (e.g., $+5\%$ or -5%). To ensure a consistent comparison of model performance across error levels, NDVI values from the same years were added in the same direction (positive or negative) of errors. Fig. 7 shows the modeling results using a 10-year time window. Other time windows are not displayed because they demonstrated similar patterns as those generated for the 10-year window. Specifically, the model goodness-of-fit (R^2) decreased remarkably in tandem with the increase of error. However, model parameters remained relatively stable (a: 0.17–0.23; b: 0.29–0.38), indicating a high resistance to NDVI errors. It is therefore meaningful and relatively robust relying on model parameters a and b to detect rubber plantations.

In tropical and subtropical regions, remote sensing data quality is often affected by cloud cover or fog inundation causing unexpected low NDVI values in the time series. Such low values (NDVI < 0.4) are similar to those collected from the starting year of rubber tree cultivation. Particularly if this 'spurious' candidate occurs in the middle of a rubber NDVI time series, the actual starting year (defining rubber tree age) may not be identified. Here, we based our tests on a rubber NDVI time series simulated with the average a and b values 0.23 and 0.31 as derived from the training samples (Table 1). We purposely reduced NDVI values to 0.2 at ages 2, 4, 6 and 8, respectively. Then, we fitted the tree growth model within all the possible time windows, treating 0.2 as the first year NDVI observation (Fig. 8). Results showed that the variation (standard deviation) of parameter a was relatively large, ranging from 0.05 to 0.09, which were higher than the parameter standard deviation values used in this study (Table 1). In out tests, higher variation occurred when the spurious candidate was closer to the stage of higher tree maturity (a1, a2 and a3 in Fig. 8). In case a4 (Fig. 8), only one time window could be evaluated. a was found to be large (0.62), which was almost twice of the maximum value of a from rubber stand training samples (0.34; Table 1), was apparently outside of the parameter range

as defined by this study (Table 1). Hence, the model showed the capacity to identify spurious candidates that may occur at various time steps in a tree growth NDVI trajectory.

3.3. Age estimation of rubber plantations

This study produced two types of maps, including the spatial distribution of rubber plantations and the associated tree age estimates. Overall, the proposed mapping approach achieved an accuracy of 87.00% for identifying rubber plantations, with kappa statistic of 0.75. Rubber and non-rubber land cover both achieved over 80% user's and producer's accuracies (Table 2), which had comparable or slightly lower performance as those reported in previous rubber tree mapping projects using Landsat imagery (e.g., Li and Fox, 2011; Dong et al., 2013; Kou et al., 2015).

On average, the age of rubber stands was estimated with an error (RMSE) of 1.53 years. Fig. 9 shows a comparison of estimated *versus* reference rubber tree age, where larger bubbles represent more validation samples overlaid on the corresponding spots. The errors did not show noticeable biases at specific ages, including the pre-mature tree growing stage (e.g., age < 7 years old) that is usually challenging to estimate (Chen et al., 2012; Dong et al., 2013). Most of the errors occurred within a two-year range, possibly caused by inaccurate estimation of the starting year of rubber tree cultivation. Specifically, underestimation was possibly resulting from the small canopy cover of young rubber trees in the area, where the spectral reflectance was dominated by bare soil causing NDVI values to be lower than 0.4. Overestimation was partially explained by the outcome of dense grass/shrubs or nonrubber crops covering the land prior to rubber tree cultivation making NDVI values higher than 0.4. While errors remained, they were relatively small and consistent across young, middle-age, and mature rubber plantations. To the best of our knowledge, such level of accuracy was rarely achieved in earlier studies. For example, Chen et al. (2012) applied Landsat TM data to estimate the stand age of rubber plantations
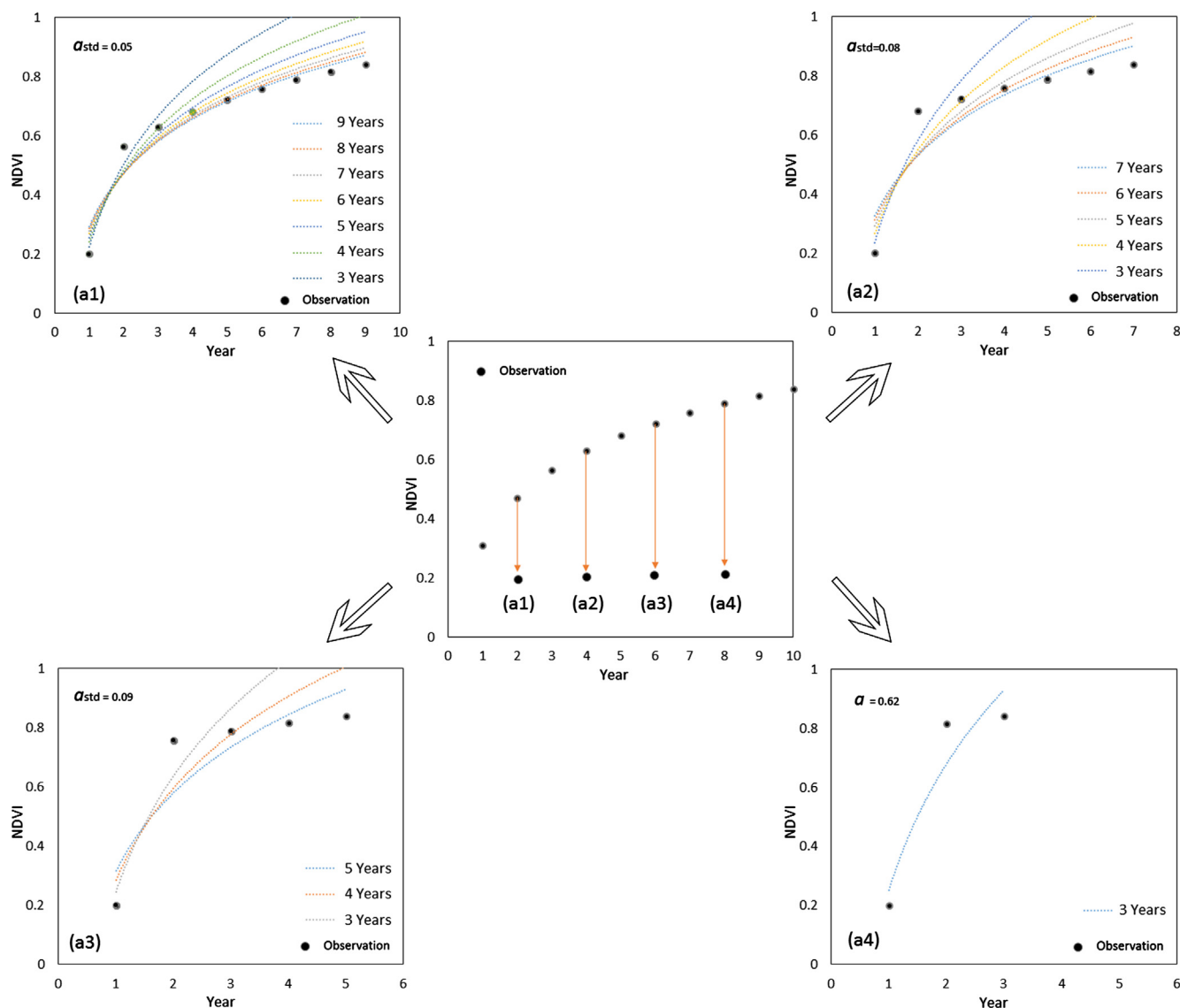
Fig. 8. The capacity of tree growth modeling to capture spurious initial year candidates (with low NDVI values) occurring at various time steps.

Table 2
Confusion matrix and kappa statistic of the rubber mapping result.

User class	Reference class		Total	User's accuracy
	Rubber plantation	Non-rubber land cover		
Rubber plantation	40	6	46	86.96%
Non-rubber land cover	7	47	54	87.04%
Total	47	53	100	
Producer's accuracy	85.11%	88.68%		

Overall accuracy = 87.00%; Kappa statistic = 0.75.

in Hainan, China. They compared different variable inputs (e.g., spectral signature, vegetation indices and tasseled cap components) using regression techniques. The best model achieved an error of 5.96 years. Using the same type Landsat TM data, Suratman et al. (2004) achieved estimation errors from 6.4 to 8.2 years. In a Yunan study site that is close to our mapping area, Kou et al. (2015) integrated both Landsat time series and L-band PLASAR images to estimate rubber stand age. Instead of treating age as a continuous variable, they categorized age

into three groups (≤5, 6–10, > 10 years), which achieved accuracies between 80% and 90%. Similarly, Li and Fox (2012) applied MODIS time series to extract two groups of rubber plantations: young (< 4 years) and mature rubber trees (≥4 years). While the results demonstrated accuracies over 97%, both the age classes and map spatial resolution (250 m) were coarse.

We generated a rubber plantation age map for the entire study area (Fig. 10). The final year of the evaluated NDVI time series 2015 was treated as the current date. Because our approach required at least three years of NDVI observations to fit the tree growth model, the youngest plantations were estimated at the age of 3 years old. The oldest were 15 years old, as we did not use NDVI observations prior to 2001. In general, the age map confirmed the reported intensive rubber cultivation activities in China, which were initiated earlier than its neighbors Myanmar and Laos (Smajgl et al., 2015; Liu et al., 2016). A spatial expansion pattern was clearly observed in a border area between China and Myanmar, where young rubber trees (cyan-blue) were recently planted adjacent to the more mature plantations (red-yellow) located in the north (Fig. 10). Our findings confirmed the recent political and economic reforms in Myanmar and Laos, aiming to attract foreign investors (e.g., China and Thailand) through allocating land concessions (Woods, 2012; Ziegler et al., 2009; Liu et al., 2016). While young
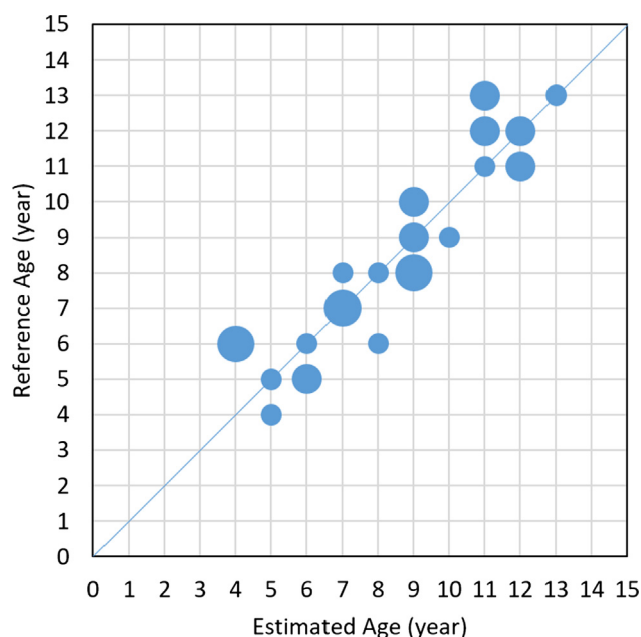
Fig. 9. Estimated *versus* reference age, where larger bubbles represent more samples overlaid on the corresponding spots.

plantations were also discovered in Laos, they were found to follow a more scattered distribution pattern than in the other two nations, possibly the compound effects of natural environment, politics, and socioeconomics. In many areas, we further discovered a spatial pattern of dense rubber plantations in urban peripheries (e.g., the bottom-left region in Fig. 10), which was likely a strategy for cost-effective

transportation and logistics since rubber tapping is labor intensive (Mann, 2009).

The global rubber market prices rose significantly in the 2000s jumping from less than 25 to over 280 cents per pound (IndexMundi, 2017), which has been the driving force behind the rapid expansion of rubber plantations in mainland Southeast Asia (Li and Fox, 2012). It was also evidenced in our study area, where the estimated rubber tree expansion followed the similar pattern of rubber market price change (Fig. 11). A time-lag effect was also observed, where the pace of rubber expansion seemed to reflect the change in rubber market price a couple of years behind.

4. Conclusions

This study developed an integrated pixel- and object-based tree growth model using Landsat annual time series to estimate the stand age of rubber plantations. The performance of the model was evaluated in a 21,115 km^2 tri-border region along the junction of China, Myanmar and Laos from three aspects. First, the integration of pixel- and object-based image analysis showed superior performance in building yearly NDVI time series that resulted in apparent tree growth trajectories. Compared to the classic pixel-based approach, our method took into consideration the contextual information in rubber tree stands, reducing spectral noise from background soil and vegetation. Second, model sensitivity analysis was performed using real NDVI observations and through simulations. We found that model parameters (*a* and *b* in Eq. (1) remained relatively stable during the analysis, making stand age estimation robust to outliers. The application of the proposed model to the entire study area resulted in an average age estimation error of 1.53 years. Third, our model demonstrated consistent performance across young, middle-age, and mature rubber plantations. While developed and evaluated in one study area, the model proved the feasibility of integrating image time series and tree growth modeling to
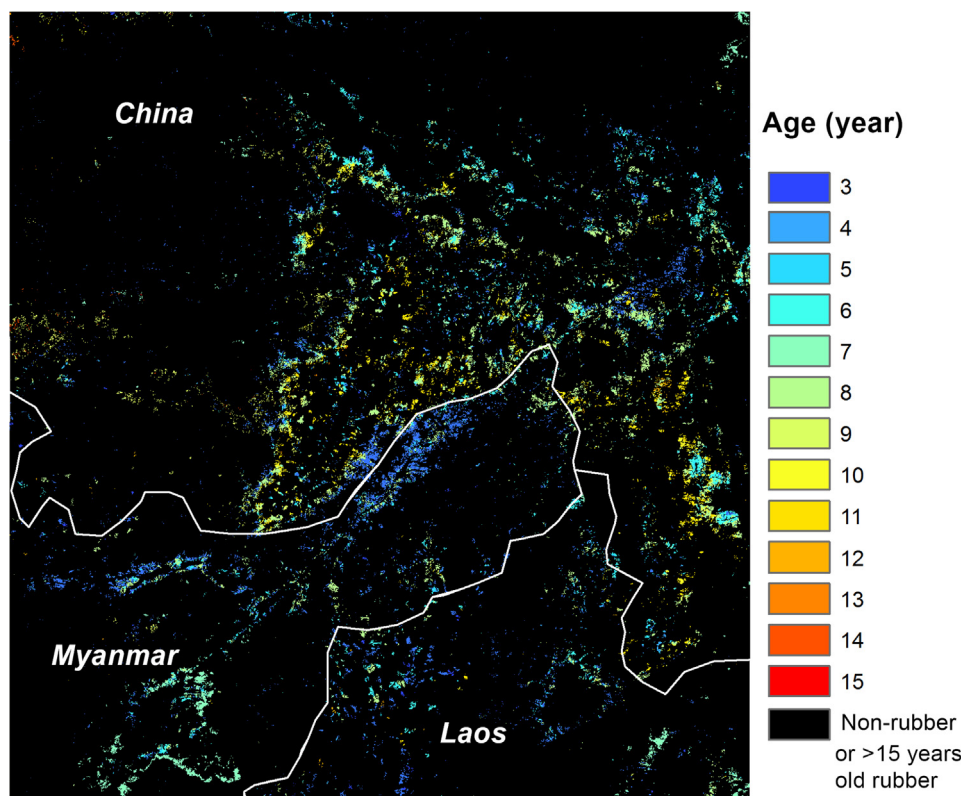

Fig. 10. Age estimation of rubber plantations in a tri-border region along the junction of China, Myanmar and Laos. White lines represent the country borders.
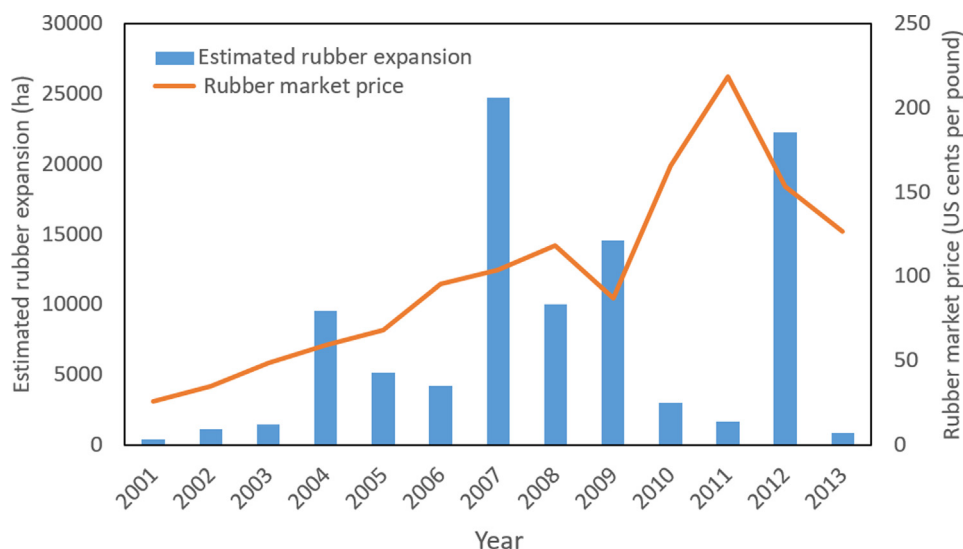
Fig. 11. Comparison between rubber expansions in our study area and global rubber market prices from 2001 to 2013.

estimate the stand age of a dominant plantation crop of rubber. In regions covered by mixed plant species that may show similar tree growth trajectories (e.g., oil palm *versus* rubber trees), age estimation may be facilitated by extending our model to incorporate fine-scale phenological variation from multi-source time series (e.g., Sentinel-2 and ASTER).

Acknowledgements

References

Alton, C., Bluhm, D., Sannanikone, S., 2005. Para Rubber in Northern Laos: The Case of Luangnamth. Lao-German Program, Rural Development in Mountainous Areas of Northern Laos, Vientiane.

Blagodatsky, S., Xu, J., Cadisch, G., 2016. Carbon balance of rubber (*Hevea brasiliensis*) plantations: A review of uncertainties at plot, landscape and production level. Agric. Ecosyst. Environ. 221, 8–19.

Blaschke, T., Hay, G.J., Kelly, M., et al., 2014. Geographic Object-Based Image Analysis – Towards a new paradigm. ISPRS J. Photogramm. Remote Sens. 87, 180–191.

Chen, B., Cao, J., Wang, J., Wu, Z., Tao, Z., Chen, J., Yang, C., Xie, G., 2012. Estimation of rubber stand age in typhoon and chilling injury afflicted area with Landsat TM data: A case study in Hainan Island, China. For. Ecol. Manage. 274, 222–230.

Chen, G., Metz, M.R., Rizzo, D.M., Dillon, W.W., Meentemeyer, R.K., 2015. Object-based assessment of burn severity in diseased forests using high-spatial and high-spectral resolution MASTER airborne imagery. ISPRS J. Photogramm. Remote Sens. 102, 38–47.

Chen, G., Hay, G.J., Castilla, G., St-Onge, B., Powers, R., 2011. A multiscale geographic object-based image analysis (GEOBIA) to estimate lidar-measured forest canopy height using Quickbird imagery. Int. J. Geograph. Informat. Sci. 25, 877–893.

Chen, G., Weng, Q., 2018. Special issue: Remote sensing of our changing landscapes with Geographic Object-based Image Analysis (GEOBIA). GISci. Remote Sens. 55, 155–158.

Chen, G., Weng, Q., Hay, G.J., He, Y., 2018. Geographic Object-based Image Analysis (GEOBIA): Emerging trends and future opportunities. GISci. Remote Sens. 55, 159–182.

Chen, G., Zhao, K., Powers, R.P., 2014a. Assessment of the image misregistration effects on object-based change detection. ISPRS J. Photogramm. Remote Sens. 87, 19–27.

Chen, J., Ban, Y., Li, S., 2014b. China: Open access to Earth land-cover map. Nature 514, 434–444.

Drăguţ, L., Tiede, D., Levick, S.R., 2010. ESP: a tool to estimate scale parameter for multiresolution image segmentation of remotely sensed data. Int. J. Geograph. Informat. Sci. 24, 859–871.

Dong, J., Xiao, X., Chen, B., Torbick, N., Jin, C., Zhang, G., Biradar, C., 2013. Mapping deciduous rubber plantations through integration of PALSAR and multi-temporal Landsat imagery. Remote Sens. Environ. 134, 392–402.

Dong, J., Xiao, X., Sheldon, S., Biradar, C., Xie, G., 2012. Mapping tropical forests and

rubber plantations in complex landscapes by integrating PALSAR and MODIS imagery. ISPRS J. Photogramm. Remote Sens. 74, 20–33.

Fox, J., Castella, J., 2013. Expansion of rubber (*Hevea brasiliensis*) in Mainland Southeast Asia: what are the prospects for smallholders? J. Peasant Stud. 40, 155–170.

Giambelluca, T.W., Mudd, R.G., Liu, W., et al., 2016. Evapotranspiration of rubber (*Hevea brasiliensis*) cultivated at two plantation sites in Southeast Asia. Water Resour. Res. 52, 660–679.

Grogan, K., Pflugmacher, D., Hostert, P., Kennedy, R., Fensholt, R., 2015. Cross-border forest disturbance and the role of natural rubber in mainland Southeast Asia using annual Landsat time series. Remote Sens. Environ. 169, 438–453.

IndexMundi, 2017. Rubber Monthly Price. Available online: http://www.indexmundi.com/commodities/?commodity=rubber.

Kou, W., Xiao, X., Dong, J., Gan, S., Zhai, D., Zhang, G., Qing, Y., Li, L., 2015. Mapping deciduous rubber plantation areas and stand ages with PALSAR and Landsat images. Remote Sens. 7, 1048–1073.

Kumagai, T., Mudd, R.G., Giambelluca, T.W., et al., 2015. How do rubber (Hevea brasiliensis) plantations behave under seasonal water stress in northeastern Thailand and central Cambodia? Agric. For. Meteorol. 213, 10–22.

Li, Z., Fox, J.M., 2011. Rubber tree distribution mapping in Northeast Thailand. Int. J. Geosci. 2, 573–584.

Li, Z., Fox, J.M., 2012. Mapping rubber tree growth in mainland Southeast Asia using time-series MODIS 250 m NDVI and statistical data. Appl. Geogr. 32, 420–432.

Liu, X., Feng, Z., Jiang, L., Li, P., Liao, C., Yang, Y., You, Z., 2013. Spatial-temporal analysis of rubber plantation and its relationship with topographical factors in the border region of China, Laos and Myanmar. Acta Geograph. Sin. 68, 1432–1446.

Liu, X., Jiang, L., Feng, Z., Li, P., 2016. Rubber plantation expansion related land use change along the Laos-China border region. Sustainability 8, 1011.

Mann, C.C., 2009. Addicted to Rubber. Science 325, 564–566.

Payne, A.R., 1962. The dynamic properties of carbon black-loaded natural rubber vulcanizates. Part I. J. Appl. Polym. Sci. 6, 57–63.

Simorangkir, D., Moore, P., Haase, N., Ng, G., 2002. Workshop Report: Land clearing on degraded lands for plantation development. In: A Workshop on Economics of Fire Use in Agriculture and Forest Plantations (Kuching: Fire Fight South East Asia, IUCN, and WWF).

Senf, C., Pflugmacher, D., van der Linden, S., Hostert, P., 2013. Mapping rubber plantations and natural forests in Xishuangbanna (Southwest China) using multi-spectral phenological metrics from MODIS time series. Remote Sens. 5, 2795–2812.

Smajgl, A., Xu, J., Egan, S., Yi, Z.-F., Ward, J., Su, Y., 2015. Assessing the effectiveness of payments for ecosystem services for diversifying rubber in Yunnan, China. Environ. Modell. Software 69, 187–195.

Suratman, M.N., Bull, G.Q., Leckie, D.G., Lemay, V.M., Marshall, P.L., Mispan, M.R., 2004. Prediction models for estimating the area volume, and age of rubber (*Hevea brasiliensis*) plantations in Malaysia using Landsat TM data. Int. For. Rev. 6, 1–12.

Trisasongko, B.H., 2017. Mapping stand age of rubber plantation using ALOS-2 polarimetric SAR data. Eur. J. Remote Sens. 50, 64–76.

Woods, K., 2012. The Political Ecology of Rubber Production in Myanmar: An Overview. Retrieved from: http://www.burmalibrary.org/docs20/The_Political_Ecology_of_Rubber_Production_in_Myanmar.pdf.

Xu, J., Grumbine, R., Beckschaefer, P., 2013. Landscape transformation and use of ecological and socioeconomic indicators in Xishuangbanna, Southwest China, Mekong Region. Ecol. Ind. 36, 749e756.

Yi, Z.-F., Wong, G., Cannon, C.H., Xu, J., Beckschäfer, P., Swetnam, R.D., 2014. Can carbon-trading schemes help to protect China's most diverse forest ecosystems? A case study from Xishuangbanna, Yunnan. Land Use Policy 38, 646–656.

Zhai, D.L., Cannon, C.H., Slik, J.W.F., Zhang, C.P., Dai, Z.C., 2012. Rubber and pulp plantations represent a double threat to Hainan's natural tropical forests. J. Environ. Manage. 96, 64–73.

Ziegler, A.D., Fox, J.M., Xu, J., 2009. The rubber juggernaut. Science 324, 1024–1025.

Zomer, R.J., Trabucco, A., Wang, M., Lang, R., Chen, H., Metzger, M.J., Smajgl, A., Beckschäfer, P., Xu, J., 2014. Environmental stratification to model climate change impacts on biodiversity and rubber production in Xishuangbanna, Yunnan, China. Biol. Conserv. 170, 264–273.